STM JOURNALS

Journal of
Polymer & Composites

ISSN: 2321-2810 (Online)
ISSN: 2321-8525 (Print)
Volume 13, Special Issue 1, 2025
DOI (Journal): 10.37591/JoPC

https://journals.stmjournals.com/jopc

Research JoPC

Synthesis and Photoluminescence Dynamics of Europium (III) and Terbium (III) Co-doped of $GdSrAl_3O_7$ Color-Tunable Nanophosphors

Deepika Dhaterwal[1], Mahesh Matoria[2], Annu Dalal[3], Surender Kumar[4], Sonika Singh[5,*]

Abstract

A series of Europium (III) and Terbium (III) co-doped $GdSrAl_3O_7$ color-tunable nanophosphors were synthesized by a simplistic, streamlined and self-propagating, urea-assisted solution combustion synthesis process. The structural and luminescence characteristics of synthesized Eu^{3+}/Tb^{3+} co-doped Gadolinium Strontium Aluminate nanocrystalline phosphors were validated using powder X- ray diffraction (PXRD), scanning electron microscopy (SEM), transmission electron microscopy (TEM), energy dispersive X- ray analysis (EDAX), and photoluminescence spectra studies. The morphological studies revealed that the synthesized co-doped phosphor crystals seemed to be agglomerated spherical-shaped porous nanocrystalline particles with interconnected boundaries. Through diffuse reflectance (DR) spectroscopy, the optical band gap values for nanocrystalline phosphors were also studied. The simultaneous presence of these two rare earth ions may provide specific luminous assets, including efficient energy transfer along with controlled emissions. The detailed analysis of the photoluminescence excitation (PLE) and photoluminescence emission (PL) spectra of Europium (III) and Terbium (III) co-doped $GdSrAl_3O_7$ revealed that Tb^{3+} effectually sensitized Eu^{3+} ion and that the energy transfer could be precisely controlled to achieve color- tunable emission by varying the proportions of doped ions. The non- radiant energy loss i.e. concentration quenching phenomenon was also probed in detail. Additionally, by using their emission data, colorimetric traits including Commission International de I'Eclairage 1931 color coordinates, color purity (CP), and correlated color temperature (CCT) were also obtained. The photometric properties of developed nanocrystalline co-doped phosphor materials introduce new prospects and layout potentials for upgraded luminous materials that can be used in field emission displays, solid- state technologies, multicolor display applications and a variety of illumination strategies.

***Author for Correspondence**
Sonika Singh

[1]Research Scholar, Department of Chemistry, Chaudhary Bansi Lal University, Bhiwani, Haryana, India
[2]Research Scholar, Department of Chemistry, Chaudhary Bansi Lal University, Bhiwani, Haryana, India
[3]Assistant Professor, Department of Chemistry, Chaudhary Bansi Lal University, Bhiwani, Haryana, India
[4]Professor, Department of Chemistry, Chaudhary Bansi Lal University, Bhiwani, Haryana, India
[5]Assistant Professor, Department of Chemistry, Chaudhary Bansi Lal University, Bhiwani, Haryana, India

Received Date: August 05, 2024
Accepted Date: November 14, 2024
Published Date: December 10, 2024

Citation: Deepika Dhaterwal, Mahesh Matoria, Annu Dalal, Surender Kumar, Sonika Singh. Synthesis and Photoluminescence Dynamics of Europium (III) and Terbium (III) Co-doped of $GdSrAl_3O_7$ Color-Tunable Nanophosphors. Journal of Polymer & Composites, 2025, 13(Special Issue 1): S1069–S1082p.

Keywords: Solution combustion, nanocrystalline, phosphors, photoluminescence, color coordinates

INTRODUCTION

The field of nanostructured luminous materials has received lots of interest recently because of their diverse potential in bio-imaging, illumination, energy composites, photocatalysis or display systems. Rare-earth enriched nanophosphors have been unique among these nanostructured luminescent substances because of their upgraded optical, electrical, structural, or chemical features, good luminous efficiency and diverse emission colors resulting from different dopants. Also, the doping and co-doping of rare earth ions in nanocrystalline phosphors improves energy efficiency, facilitating the incorporation of these materials in energy conversion and storage devices

such supercapacitors, solar panels, and batteries [1–8]. A vital component impacting luminescent materials effectiveness comprises the host matrix. In light of the robust absorption of ultraviolet radiation and remarkable optical damaging threshold of the aluminate-based melilite $ABAl_3O_7$ (A= Ba/Sr/Ca and B = La/Gd/Y) group of inorganic materials, it appears to be an attractive luminous host for doping of the different rare earth ions. The host matrix gadolinium strontium aluminate oxide ($GdSrAl_3O_7$) has revealed significant potential due to its remarkable chemical endurance, small phonon energy, and outstanding thermal durability [9–11]. $GdSrAl_3O_7$ doped with Eu^{3+} ion ordinarily produces red emission, whereas $GdSrAl_3O_7$:Tb^{3+} reveal green emission when subjected to ultraviolet (UV) stimuli [10,12]. This host has been envisaged to exhibit a tunability of hues resulting from the co-doping of Terbium (III) and Europium (III) and the precise tuning of the dopant proportions. Numerous investigations have centered on the preparation and structural content of rare-earth-rich melilite families [11,13,14]. $GdSrAl_3O_7$, a sort of aluminate, was selected as the substrate matrix in this study, as only a few reports on luminescent studies of Tb^{3+} and Eu^{3+} doped $GdSrAl_3O_7$ phosphor prepared via sol-gel method [12], and solution combustion method [10,15] have been reported in literature. However, there were no available studies in the literature to date addressing the possible energy transfer process and the impact of Eu^{3+}/Tb^{3+} co-doping on the luminescence attributes of $GdSrAl_3O_7$. In this work, $Gd_{0.99}Eu_{0.01}SrAl_3O_7$, $Gd_{0.99}Tb_{0.01}SrAl_3O_7$ and a series of $Gd_{0.99-x}Eu_xTb_{0.01}SrAl_3O_7$ (x = 0.01 to 0.07 mol) co-doped crystalline nanophosphors were synthesized through an easy-to-use, one-step, self-propagating, low-temperature solution combustion process. A thorough analysis was conducted on the structure, energy band gap, photoluminescence, and color tunable attributes. The obtained results suggested that the generated $Gd_{0.99-x}Eu_xTb_{0.01}SrAl_3O_7$ (x = 0, 0.01 to 0.07 mol) nanocrystalline luminous substances exhibited tunable emissions ranging from light green→ orange→ orange-red→ dark red color. Their intense emission and tunable luminous hue render it ideal to use in the domains of sophisticated lighting, optical devices, colored light emitting diodes, photonic devices and displays.

EXPERIMENTAL

Synthesis Method

In order to fabricate a series of Eu^{3+}/Tb^{3+} ions doped and co-doped $GdSrAl_3O_7$ nanophosphors using one-step, self-propagating, low-temperature solution combustion process, homogeneous aqueous mixtures containing metal nitrates, including gadolinium, stron tium, aluminum, europium, and terbium nitrates, were formed. With the objective of producing the appropriate composition of $GdSrAl_3O_7$ with Eu^{3+} and Tb^{3+} ions, the metal nitrates were dissolved in minimum amount of deionized water in proper proportions. A stoichiometric amount of fuel (urea) was added to the resulting mixtures in order to facilitate combustion. The resulting mixtures were carefully stirred to make homogeneous solutions. The beakers with an evenly distributed clear solution were put in the furnace, which was preheated and sustained at 500°C [15–17]. The solution ignites spontaneously and burns because of an immediate exothermic reaction triggered by the furnace's heat. The gaseous substances, notably carbon dioxide and nitrogen, emerge during this procedure, which results in voluminous, fluffy substances. After the process of combustion completes (within 5-7min), the resulting substances were allowed to cool down to ambient temperature. The following is the fundamental chemical step that led to the doped/co-doped $Gd_{1-x-y}SrAl_3O_7$:xEu^{3+}/yTb^{3+} nanocrystalline luminescent materials:

$(1\text{-}x\text{-}y)Gd(NO_3)_3.6H_2O + Sr(NO_3)_2 + xEu(NO_3)_3.6H_2O + yTb(NO_3)_3.5H_2O + Al(NO_3)_3.9H_2O + NH_2CONH_2$ (urea) → $Gd_{1-x-y}SrAl3O7$: $xEu3^{+}$/yTb^{3+} + volatile substances

Here (x = 0.01 mol, y = 0), (x = 0, y = 0.01 mol), and (x = 0.01 to 0.07mol, y = 0.01 mol). In order to enhance the crystallinity and eliminate any residual impurities, the resultant powders were sintered in a crucible at 550°C (1h) [10,15]. The compounds that were collected as solid crystalline phosphors were retained for further investigation within a desiccator.

Characterization of Co-doped $Gd_{1-x-y}SrAl_3O_7$: xEu^{3+}/yTb^{3+} Crystalline Nanophosphors

The obtained $Gd_{1-x-y}SrAl_3O_7$:xEu^{3+}/yTb^{3+} luminescent compounds crystallographic phase investigation was assessed using a Rigaku Ultima IV X-Ray powder diffractometer. Both the field emission scanning electron microscopy (FE-SEM) and transmission electron microscopy (TEM)

techniques were utilized for analysing their interface attributes and grains dimensions of synthesized co-doped nanophosphors. Energy dispersive X-ray analysis (EDAX) was leveraged to quantitatively pinpoint the constituents of fabricated phosphors. With $BaSO_4$ as a reference material, the band gap values of produced co-doped nanophosphors were studied using Shimadzu UV-3600 plus UV-Vis-NIR spectrophotometer. A HORIBA fluorescence spectrophotometer equipped with xenon light was adopted to perform the luminescence studies. The created doped/co-doped $Gd_{1-x-y}SrAl_3O_7{:}xEu^{3+}/yTb^{3+}$ nanocrystalline luminous samples, Commission International de I'Eclairage 1931 (CIE) color coordinates (x, y) along with other relevant photometric attributes were also ascertained by studying their photoluminescent results. The characterizations listed above were carried out at ambient temperature.

RESULTS AND DISCUSSION

Structural and Morphological Aspects Probes

The diffraction pattern study was utilized to analyse the phase uniformity and basic framework traits of the synthesised co-doped $Gd_{0.93}Eu_{0.06}Tb_{0.01}SrAl_3O_7$ crystalline luminescent material. The XRD pattern with the standard JCPDS card (50-1817) depicted in Figure 1a, revealed the emergence of crystalline and pure tetragonal phase of $Gd_{0.93}Eu_{0.06}Tb_{0.01}SrAl_3O_7$ co-doped phosphor at 550°C [10].

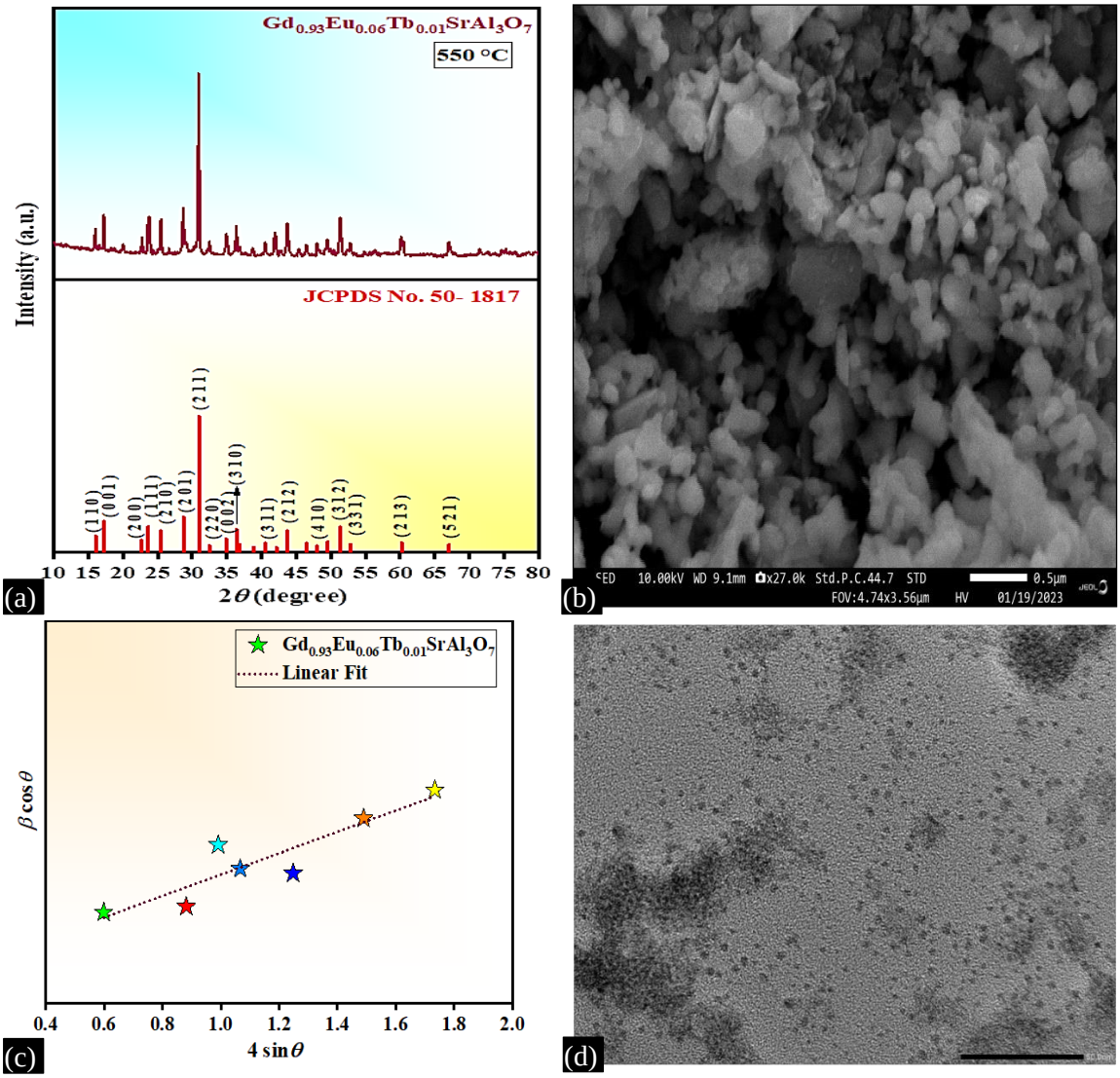

Figure 1. (a) XRD pattern, (b) W-H plot, (c) FE-SEM, and (d) TEM images of $Gd_{0.93}Eu_{0.06}Tb_{0.01}SrAl_3O_7$ phosphor.

It was feasible to precisely pinpoint the tetragonal phase of Eu^{3+}/Tb^{3+} co-doped $GdSrAl_3O_7$ by simply analysing the entire peak patterns of the co-doped phosphor sintered at 550°C. No spikes representing additional phases were discernible at this sintering temperature, which suggests the formation of single phased co-doped $Gd_{0.93}Eu_{0.06}Tb_{0.01}SrAl_3O_7$ crystalline luminescent material. The XRD data of Europium (III) and Terbium (III) ions co-doped in the $GdSrAl_3O_7$ host lattice appropriately matched the standard JCPDS card (50-1817), which suggests that the ignition energy in urea-assisted combustion seemed enough to facilitate the effective replacement of infused ions at Gd^{3+} positions in spite of retaining the same symmetry (C_s) in the host lattice [10,18]. The dopant ions have been observed to substitute for Gd^{3+} ions in the $GdSrAl_3O_7$ host lattice by virtue of their remarkably comparable dimensions and charges. More effective grasping of the swapping occurrences in $GdSrAl_3O_7$ host lattice induced by the doping of Eu^{3+} and Tb^{3+} ions was done via analyses that took account of the variation in percentage (%) radius, D_r, which has an acceptable value of less than 30% for developing precise crystal systems [19–21]. For this, the analysis process was laid out below:

$$D_r = \frac{R_h(CN) - R_d(CN)}{R_h(CN)} X\ 100\%, \quad (1)$$

Here, R_h and R_d = Ionic radius of host ion and dopant ion respectively, CN = Coordination number of particular ion. The results of Eq. 1 revealed estimated D_r (%) values of 1.235%, and 4.085% respectively, for Gd^{3+}/Tb^{3+} and Gd^{3+}/Eu^{3+}, both of which significantly below 30%. These results suggested that the host matrix's Gd^{3+} ions were substantially substituted by Eu^{3+} and Tb^{3+} ions. The nanocrystalline aspect of the fabricated co-doped $Gd_{0.93}Eu_{0.06}Tb_{0.01}SrAl_3O_7$ compound was assessed by calculating crystallite average size (D) using Scherrer's formula (Eq. 2) and Williamson-Hall (W-H) relation (Eq. 3) and additionally other figures about crystals i.e. Microstrain (ε) and Dislocation density (δ) [22–25], also measured as described below:

$$D = \frac{0.941\lambda}{\beta cos\theta} \quad (2)$$

$$\beta cos\theta = \varepsilon(4sin\theta) + \frac{0.89\lambda}{D} \quad (3)$$

$$\text{Dislocation density } (\delta) = \frac{1}{D^2} \quad (4)$$

Here, θ = Bragg's angle of an observed X-ray diffraction peak, D = crystallite average size, λ (0.154056 nm) = X-rays wavelength of CuKα radiation, β = Full width at half- maxima (FWHM) in radians. The crystallite size (D) was determined to be 40.01 nm using Scherrer's formula. A plot with a straight contour has emerged from the correlation among $4sin\theta$ (x-axis) and $\beta cos\theta$ (y-axis) as specified by Eq. 3. From the W-H plot (Figure 1b), D= 56.59 nm and strain= 0.00111, were obtained by utilizing Y-intercept of linear fit and slope, respectively. The microstrain that was taken into account in W-H method but not in Scherrer's method led to the finding that the crystallite size (D) value obtained by the W-H method was somewhat greater than obtained using Scherrer's equation [26]. Microstrain (ε) reflects matrix deformations resulting from dislocations, defects, or non-uniform stresses in the substrate's structure. This microstrain gives rise to the broadening of XRD peaks. Considering the above suggested Eq. 4, δ = 0.00031 nm^{-2} has been also ascertained.

The surface morphology, nanostructure, and distribution of dopant ions within synthesized Eu^{3+}/Tb^{3+} co-doped $GdSrAl_3O_7$ material were investigated utilizing FE-SEM, TEM, and EDAX approaches. As depicted in the FE-SEM image (Figure 1c), the tailored $Gd_{0.93}Eu_{0.06}Tb_{0.01}SrAl_3O_7$ luminescence material annealed at 550°C (1h) exhibited agglomeration with spherical-shaped porous particles having smooth surfaces and defined connection boundaries. The FE-SEM image rendered evident the existence of a couple of tiny holes induced by the volatile products release [10,27]. The tightly packed, interconnected edges of the tiny particles provide a higher surface area to volume fraction that protects it from aging. In light of the surface's smooth impact, resulting in decreased non-radiation and scattering, the efficiency of nanophosphor luminosity significantly strengthened [2,16]. The TEM result of $Gd_{0.93}Eu_{0.06}Tb_{0.01}SrAl_3O_7$ (Figure 1d), luminescent material sintered at 550°C (1h) demonstrated the randomly organized clusters of spherical-shaped tiny particles in nano range. The EDAX spectrum

(Figure 2a), demonstrates peaks corresponding to the individual constituents and an inset exhibiting the weight percentages and atomic percentage contents of each component were added as well. The EDAX mappings for all pertinent ingredients (O, Tb, Eu, Gd, Al and Sr) were illustrated in Figure 2b. The derived results exhibited the homogeneous distribution of the distinct components along with the substantial enrichment of Eu^{3+}/Tb^{3+} within the $GdSrAl_3O_7$ substrate lattice.

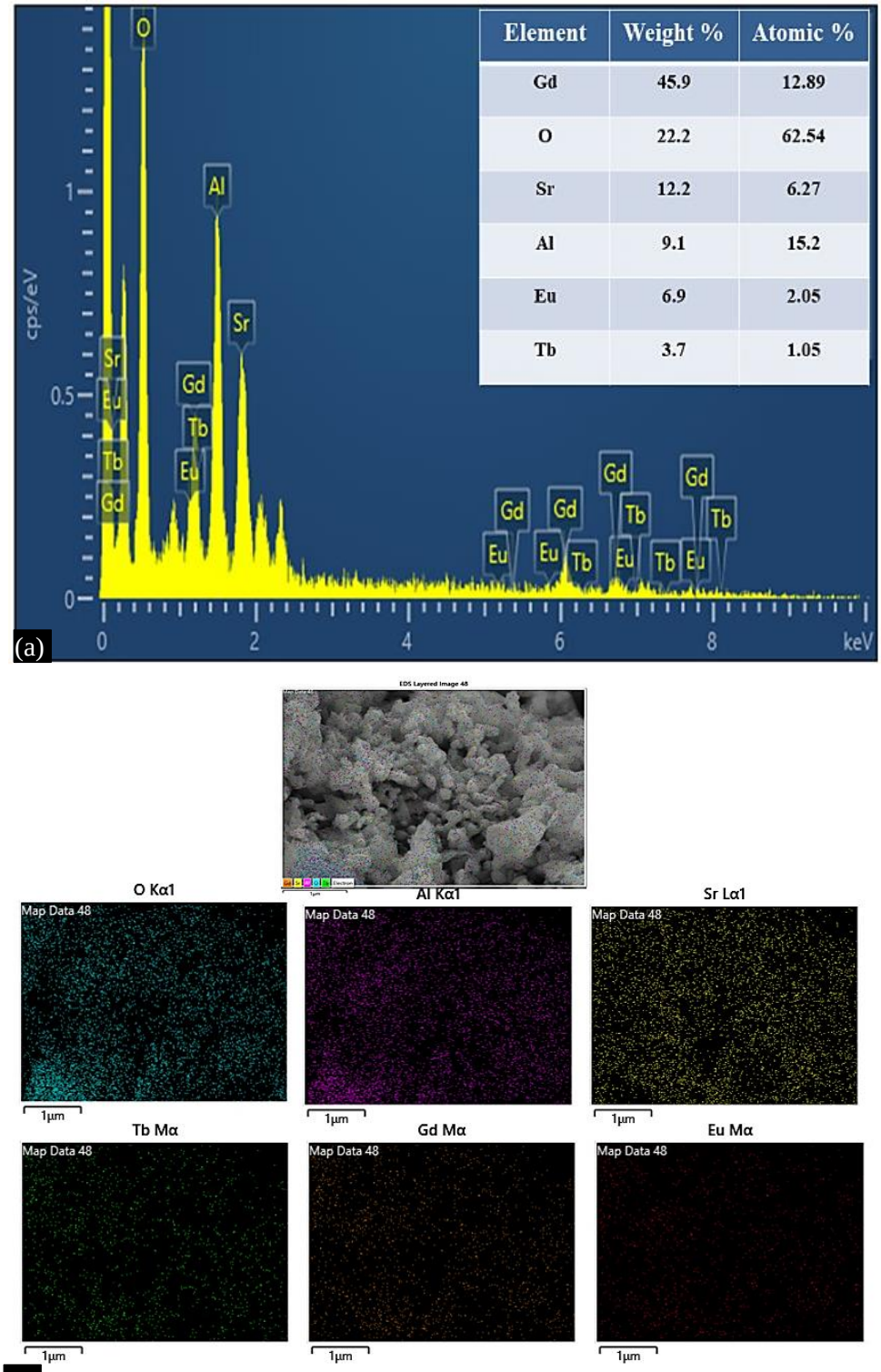

Figure 2. (a) EDAX spectra and (b) Elemental mapping of $Gd_{0.93}Eu_{0.06}Tb_{0.01}SrAl_3O_7$ phosphor

Band Gap Analysis

Diffuse reflectance (DR) spectroscopy was utilized for investigating the optical features of $Gd_{0.99}Eu_{0.01}SrAl_3O_7$, $Gd_{0.99}Tb_{0.01}SrAl_3O_7$ and $Gd_{0.99-x}Eu_xTb_{0.01}SrAl_3O_7$ (x = 0.01 to 0.07 mol) nanocrystalline phosphors. Kubelka and Munk function (Eq. 5) and Tauc's relation (Eq. 6) were applied for determining the optical band gap (E_g) of these crystalline nanomaterials [28,29].

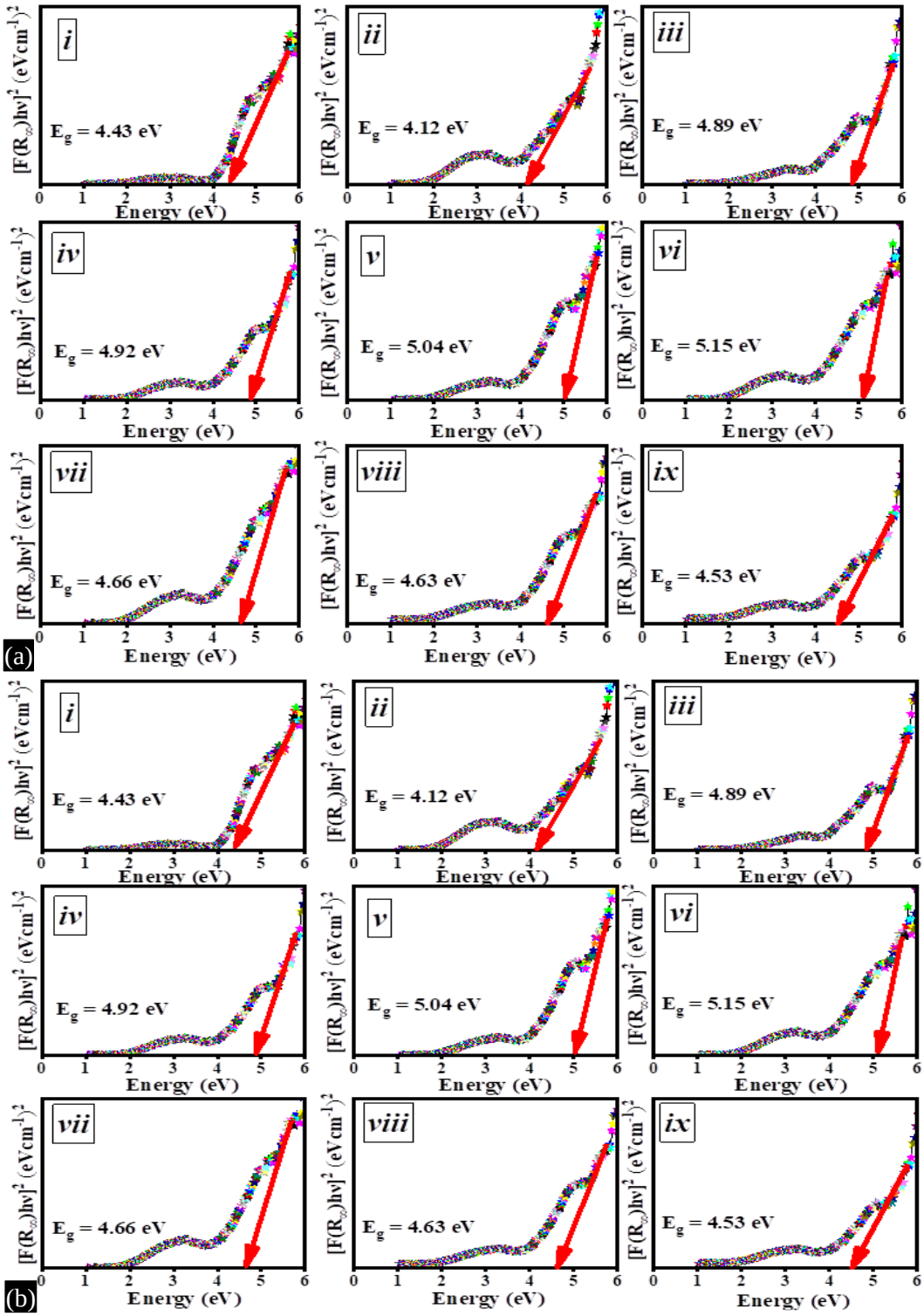

Figure 3. (a) Diffuse reflectance spectra, (b) band gap (E_g) of (i) $Gd_{0.99}Eu_{0.01}SrAl_3O_7$, (ii) $Gd_{0.99}Tb_{0.01}SrAl_3O_7$ and (iii-ix) $Gd_{0.99-x}Eu_xTb_{0.01}SrAl_3O_7$ (x = 0.01 to 0.07 mol) phosphors

$$F(R_\infty) = \frac{(1-R_\infty)^2}{2R_\infty} = \frac{K}{S} \quad (5)$$

$$[F(R_\infty)h\nu]^n = C\left(h\nu - E_g\right) \quad (6)$$

Here, $F(R_\infty)$ = Kubelka and Munk function, hν = Photon energy ($\frac{1240}{\lambda}$), n = Electronic transition nature (n = 1/2, 2, 3, and 3/2 signified direct allowed transitions, indirect allowed transitions, indirect forbidden transitions, and direct forbidden transitions, respectively), R_∞ = Sample reflection coefficient, and C, K, S = Proportionality, Absorption and Scattering constant respectively. Figure 3a and b depicted the diffuse reflectance patterns of these fabricated luminescent materials and their obtained band gaps (E_g) respectively. The derived E_g values were also tabulated in Table 1.

Table 1. The Band gap (E_g), Metallization criterion (M) and Refractive index (n) of $Gd_{0.99}Eu_{0.01}SrAl_3O_7$, $Gd_{0.99}Tb_{0.01}SrAl_3O_7$ and $Gd_{0.99-x}Eu_xTb_{0.01}SrAl_3O_7$ (x = 0.01 to 0.07 mol) nanocrystalline phosphors

Representation	Nanocrystalline Phosphor	Energy band gap (eV)	Metallization criterion (M)	Refractive index(n)
i	$Gd_{0.99}Eu_{0.01}SrAl_3O_7$	4.43	0.471	2.09
ii	$Gd_{0.99}Tb_{0.01}SrAl_3O_7$	4.12	0.454	2.15
iii	$Gd_{0.98}Eu_{0.01}Tb_{0.01}SrAl_3O_7$	4.89	0.494	2.02
iv	$Gd_{0.97}Eu_{0.02}Tb_{0.01}SrAl_3O_7$	4.92	0.496	2.01
v	$Gd_{0.96}Eu_{0.03}Tb_{0.01}SrAl_3O_7$	5.04	0.501	1.99
vi	$Gd_{0.95}Eu_{0.04}Tb_{0.01}SrAl_3O_7$	5.15	0.507	1.97
vii	$Gd_{0.94}Eu_{0.05}Tb_{0.01}SrAl_3O_7$	4.66	0.483	2.05
viii	$Gd_{0.93}Eu_{0.06}Tb_{0.01}SrAl_3O_7$	4.63	0.481	2.06
ix	$Gd_{0.92}Eu_{0.07}Tb_{0.01}SrAl_3O_7$	4.53	0.476	2.07

In light of the distinction in E_g values of co-doped $Gd_{0.99-x}Eu_xTb_{0.01}SrAl_3O_7$ and Eu^{3+} or Tb^{3+} doped $GdSrAl_3O_7$ phosphor materials, some levels of doped ions accumulation could potentially be feasible. The enhanced band gap value of $Gd_{0.99-x}Eu_xTb_{0.01}SrAl_3O_7$ nanocrystalline phosphor with an increase in Eu^{3+} ion contents was observed as a result of the Moss effect. Despite this, as the concentration of Eu^{3+} ions increases more, E_g value falls; this could occur due to dopant ion sublevels arising closer to the conduction band. Moreover, Metallization criterion (M) and Refractive index (n) of these synthesised luminescent nanomaterials were calculated using Eq. 7 and Eq. 8 (Dimitrov and Sakka's expression) respectively. The non-metallic nature of these co-doped $Gd_{0.99-x}Eu_xTb_{0.01}SrAl_3O_7$ (x = 0.01 to 0.07 mol) phosphors were demonstrated by the theoretically calculated M (M< 1, Table 1) values [20,30–33].

$$\frac{n^2-1}{n^2+2} = 1 - \sqrt{\frac{E_g}{20}} \quad (7)$$

$$M = 1\text{-}\frac{n^2-1}{n^2+2} = \sqrt{\frac{E_g}{20}} \quad (8)$$

Analysis of Photoluminescence Traits

The photoluminescence excitation (PLE) and photoluminescence emission (PL) spectra of $Gd_{0.99}Eu_{0.01}SrAl_3O_7$ and $Gd_{0.99}Tb_{0.01}SrAl_3O_7$ were depicted in Figure 4a and b respectively and all the associated transitions were tabulated in Table 2.

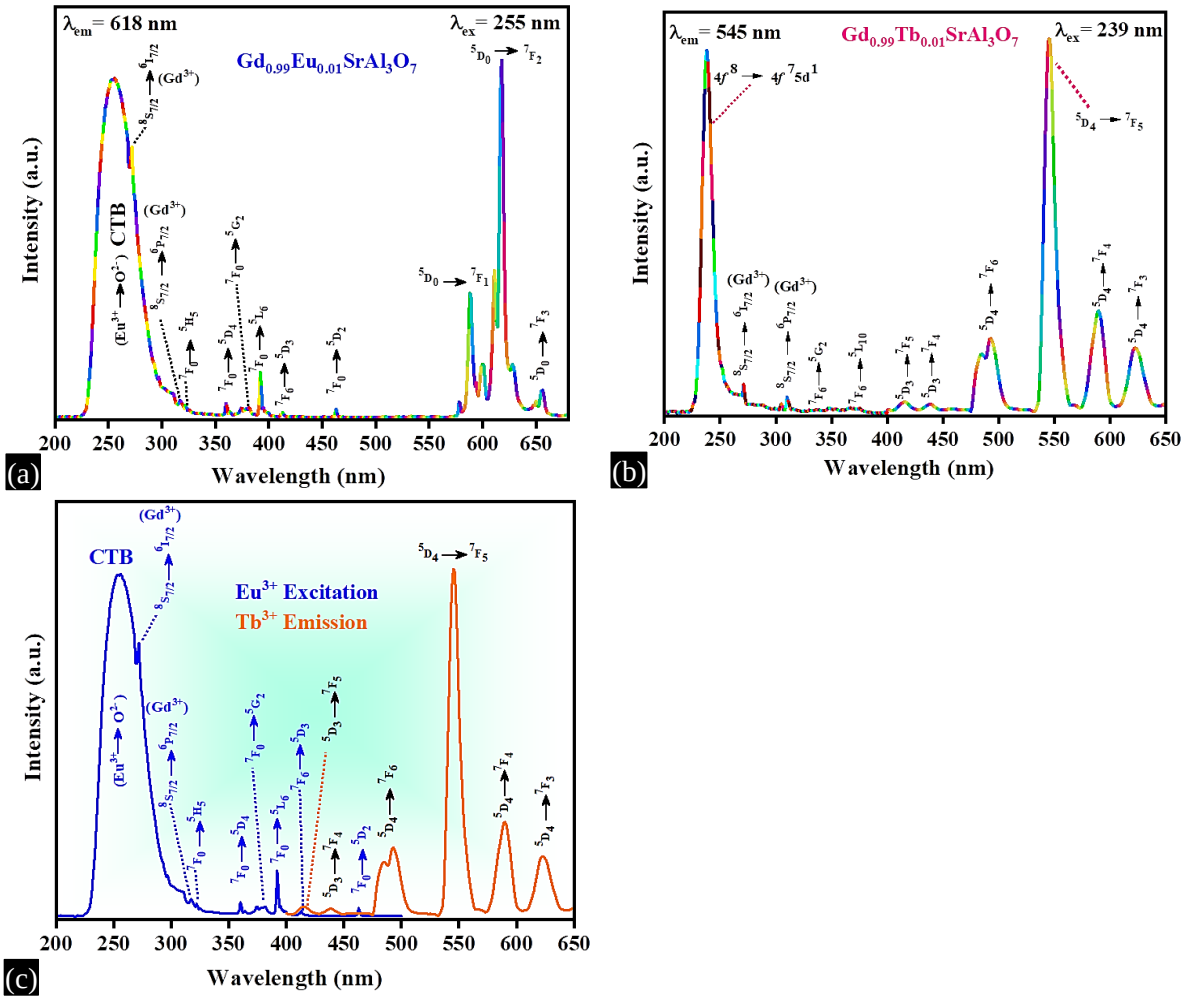

Figure 4. PLE and PL spectra of (a) $Gd_{0.99}Eu_{0.01}SrAl_3O_7$, (b) $Gd_{0.99}Tb_{0.01}SrAl_3O_7$ nanocrystalline phosphor sintered at 550°C (c) spectral overlap among Eu^{3+} excitation and Tb^{3+} emission in $GdSrAl_3O_7$ host.

Table 2. PL excitation, emission peaks and associated transitions details of $Gd_{0.99}Eu_{0.01}SrAl_3O_7$, $Gd_{0.99}Tb_{0.01}SrAl_3O_7$, and $Gd_{0.99-x}Eu_xTb_{0.01}SrAl_3O_7$ nanocrystalline phosphors

For $Gd_{0.99}Eu_{0.01}SrAl_3O_7$ nanophosphor			
Transitions	***Excitation peak wavelength (nm)***	***Transitions***	***Emission peak Wavelength (nm)***
Charge transfer (CT) band	255	$^5D_0 \rightarrow {}^7F_1$	588
$^8S_{7/2} \rightarrow {}^6I_{7/2}, {}^6P_{7/2}$	272, 314	$^5D_0 \rightarrow {}^7F_2$	618
$^7F_0 \rightarrow {}^5H_5, {}^5D_4, {}^5G_2, {}^5L_6, {}^5D_2$	322, 360, 382, 393, 462	$^5D_0 \rightarrow {}^7F_3$	656
$^7F_6 \rightarrow {}^5D_3$	412		
For $Gd_{0.99}Tb_{0.01}SrAl_3O_7$ nanophosphor			
$4f^8 \rightarrow 4f^7\,5d^1$	239	$^5D_3 \rightarrow {}^7F_5, {}^7F_4$	415, 440
$^8S_{7/2} \rightarrow {}^6I_{7/2}, {}^6P_{7/2}$	272, 314	$^5D_4 \rightarrow {}^7F_6$	491
$^7F_6 \rightarrow {}^5G_2, {}^5L_{10}$	338, 375	$^5D_4 \rightarrow {}^7F_5, {}^7F_4, {}^7F_3$	545, 593, 623
For $Gd_{0.99-x}Eu_xTb_{0.01}SrAl_3O_7$ (x = 0.01 to 0.07 mol) nanophosphors			
Charge transfer (CT) band	255	$^5D_4 \rightarrow {}^7F_5$	545
$^8S_{7/2} \rightarrow {}^6I_{7/2}, {}^6P_{7/2}$	272, 314	$^5D_0 \rightarrow {}^7F_1$	588
$^7F_0 \rightarrow {}^5H_5, {}^5D_4, {}^5G_2, {}^5L_6, {}^5D_2$	322, 360, 382, 393, 462	$^5D_0 \rightarrow {}^7F_2$	618
$^7F_6 \rightarrow {}^5D_3$	412	$^5D_0 \rightarrow {}^7F_3$	656

The small peaks observed in both excitation spectra of Eu^{3+} and Tb^{3+} doped $GdSrAl_3O_7$ correspond to $^8S_{7/2} \rightarrow {}^6I_{7/2}$ (Gd^{3+}) and $^8S_{7/2} \rightarrow {}^6P_{7/2}$ (Gd^{3+}) reflecting energy transfer from $Gd^{3+} \rightarrow RE^{3+}$($Eu^{3+}$/$Tb^{3+}$). From the emission spectrum of $Gd_{0.99}Eu_{0.01}SrAl_3O_7$ nanosample at 255 nm excitation, the observed high intensity red emission peak associated with electric-dipole transitions ($^5D_0 \rightarrow {}^7F_2$) was observed in contrast to orange-red emission peak associated to magnetic-dipole transition ($^5D_0 \rightarrow {}^7F_1$) which suggests the non-centrosymmetric arrangement of Eu^{3+} in $GdSrAl_3O_7$ host lattice [10,26,34,35]. Energy transfer has been found to have a significant role in luminous materials, both from a theoretical and practical aspect. According to Dexter theory, the preliminary need for energy transfer was effectively fulfilled as there was significant overlap revealed in PLE spectrum of Eu^{3+} ions and PL spectrum of Tb^{3+} ions (Figure 4c). Studies in the literature also suggest the energy transfer between Tb^{3+} and Eu^{3+} could take place with the help of the phonons spectrum, particularly in instances involving only slight spectral coincidence [36–39].

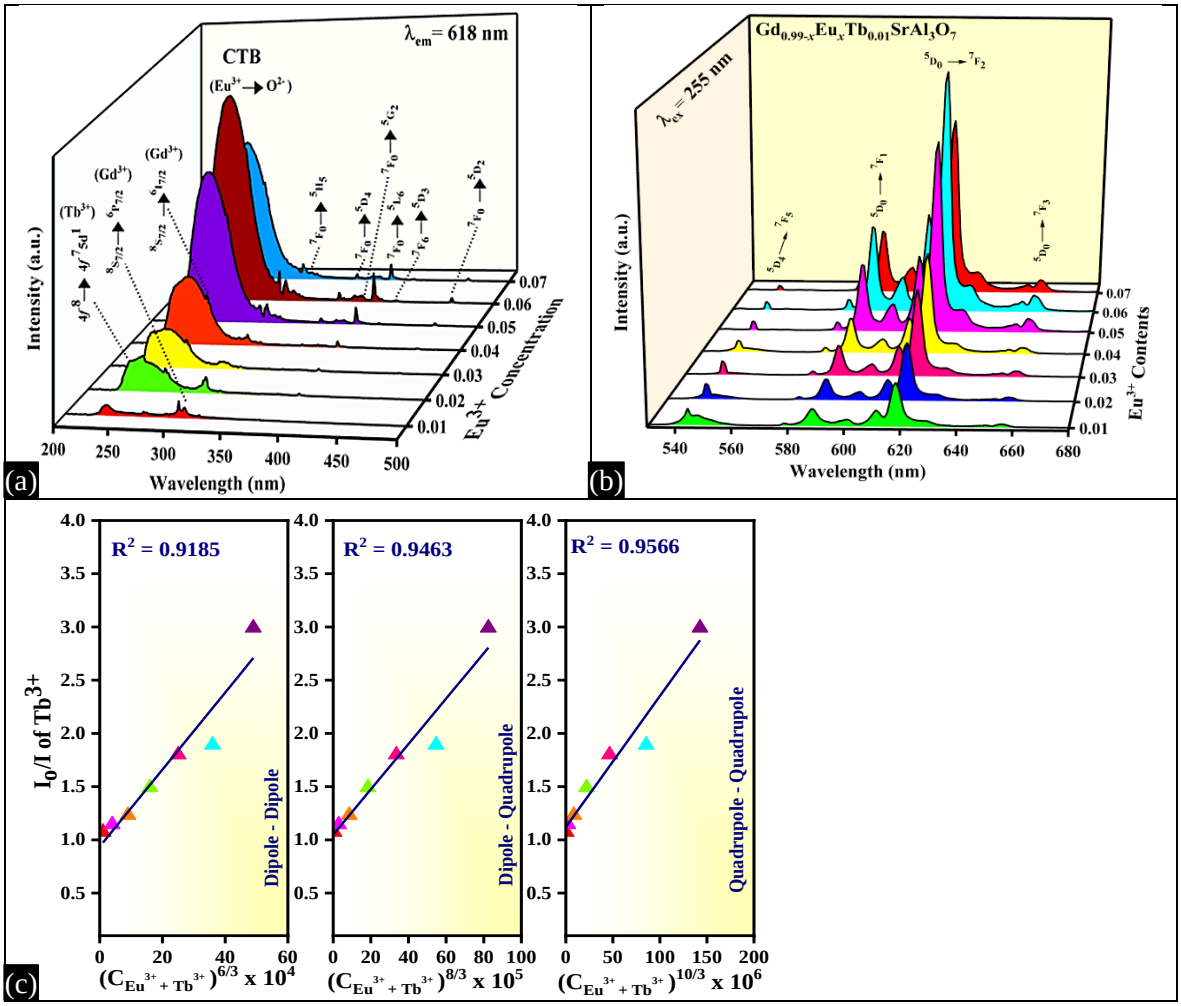

Figure 5. Collective (a) excitaion (b) emission spectra of $Gd_{0.99-x}Eu_xTb_{0.01}SrAl_3O_7$ (x = 0.01 to 0.07 mol) (c) dependence of I_o/I of Tb^{3+} on $(C_{Eu^{3+}+Tb^{3+}})^{n/3}$ for Eu^{3+}/ Tb^{3+} co-doped $GdSrAl_3O_7$ nanophosphors

In order to investigate the significant luminosity characteristics and the potential color tunability of $Gd_{0.99-x}Eu_xTb_{0.01}SrAl_3O_7$ (x= 0.01 to 0.07 mol) nanophosphors, the excitation and emission spectra of these produced co-doped phosphors were considered, as shown in Figure 5a, and additionally, Table 2 included an array of all the relevant peaks. A wide charge transfer (CT) excitation band with a maximum at 255 nm corresponding to O^{2-}-Eu^{3+} linkage, and the unique excitation peaks of Gd^{3+}, Tb^{3+} and Eu^{3+} ions (Figure 5a) were easily observed in the PLE spectra when the surveillance emission wavelength (λ_{em}) was 618 nm. The synthesized co-doped nanosamples exhibited excitation spectra that were

strikingly comparable to the excitation spectrum of $Gd_{0.99}Eu_{0.01}SrAl_3O_7$ nanocrystalline phosphors as depicted in (Figure 4a) as Tb^{3+} ions excitation band overlay with the excitation bands of Eu^{3+} ions predominantly because the intensity resulting from Tb^{3+} transitions was noticeably lesser than that of Eu^{3+} transitions. Under 255 nm excitation, the collective PL spectra (Figure 5b) of $Gd_{0.99-x}Eu_xTb_{0.01}SrAl_3O_7$ (x= 0.01 to 0.07 mol) co-doped photoluminescent materials revealed the emission peaks of Eu^{3+} ions in addition to the relatively low intensity Tb^{3+} ion emission peak at 545 nm. As demonstrated in (Figure 5b) as the amount of doped Eu^{3+} ions rose in $Gd_{0.99-x}Eu_xTb_{0.01}SrAl_3O_7$ (x = 0.01 to 0.07 mol) samples, the luminous intensity of Eu^{3+} ($^5D_0 \rightarrow {}^7F_2$) ions enhanced while the luminous intensity of Tb^{3+} ($^5D_4 \rightarrow {}^7F_5$) ions steadily dropped. Further possibility for energy transfer from $^5D_4$ (Tb^{3+}) to $^5D_0$ (Eu^{3+}) energy levels in $GdSrAl_3O_7$ matrix seems by the reduction in Tb^{3+} ion emission intensity in synthesized co-doped luminescent materials. The concentration quenching process was noticed after x = 0.06 mol in these co-doped powdered materials. This non-radiant energy loss process might occur via three pathways i.e. exchange interaction, multipolar interaction, and radiation re-absorption [40–42] . The calculated critical distance (R_c = 16.21Å) by using the following Blasse *et al. Eq.* 9 suggests that the energy transfer process amid the dopant ions is primary possible due to the multipolar interaction [21,43].

$$R_c = 2\left(\frac{3V}{4\pi x_c N}\right)^{1/3} \quad (9)$$

Where, V = volume of the unit cell, x_c = critical amount of dopant (Tb^{3+} + Eu^{3+}) ions, N = number of available sites for the dopants in a unit cell. Dexter energy transfer Eq. 10 of multipolar interaction can be used in order to better understand mechanisms of multipolar interactions between dopant ions in $GdSrAl_3O_7$ lattice [36,44] as follows:

$$\frac{\eta_0}{\eta} = C^{n/3} \quad (10)$$

Here η_0, η = sensitizer (Tb^{3+}) quantum efficiency in nonexistence of activator and with activator (Eu^{3+}), respectively, C = sum of concentration of Tb^{3+} and Eu^{3+}, and n = 6, 8, 10 values corresponding to dipole-dipole interaction, dipole-quadrupole interaction, quadrupole-quadrupole interaction respectively. With the help of Reisfeld's approximation the η_0/η, ratio value can be determined approximated from the proportion of photoluminescence intensity (I_0/I), where I and I_0 denoted the photoluminescence intensities of the sensitizer (Tb^{3+}) with and devoid of activator (Eu^{3+}), respectively [42]. The most linear tandem appeared at n = 10 as revealed in correlation plots of (I_0/I) versus $C^{n/3}$ of synthesized co-doped nanocrystalline phosphors (Figure 5c). This obtained outcome depicted the quadrupole-quadrupole interaction, among Tb^{3+} and Eu^{3+} in $GdSrAl_3O_7$ host [45]. The scheme for feasible energy transfer process in Eu^{3+}/Tb^{3+} co-doped $GdSrAl_3O_7$ phosphors was demonstrated in Figure 6a [46,47].

Study of Colorimetric Attributes

All the CIE traits i.e. the color coordinates (x, y), color-purity (CP), and the color correlated temperature (CCT) of Eu^{3+}/Tb^{3+} ions co-doped $GdSrAl_3O_7$ nanophosphors were derived from the corresponding emission data [16,48,49]. The color coordinates were calculated through MATLAB software system and the CP of these synthesized nanophosphors was determined via Eq. 11.

$$\text{Color Purity (\%)} = \frac{\sqrt{(x-x_i)^2+(y-y_i)^2}}{\sqrt{(x_d-x_i)^2+(y_d-y_i)^2}} X\ 100 \quad (11)$$

Where (x, y) = CIE color coordinates, (x_i, y_i) = white illumination coordinates (x_i = 0.31006, y_i = 0.31616) and (x_d, y_d) = CIE color coordinates associated to dominant wavelength. Also, the CCT was calculated using the empirical Mc-Camy formula (Eq. 12). Here the chromaticity epicentre is at x_e = 0.332 and y_e = 0.186 and n = (x – 0.332)/(y – 0.186). Eq.13 used to modify the chroma coordinates (x, y to u′, v′) [50].

$$CCT = -437n^3 + 3601n^2 - 6861n + 5514.3 \quad (12)$$

$$u' = \frac{4x}{-2x+12y+3} \qquad v' = \frac{9y}{-2x+12y+3} \quad (13)$$

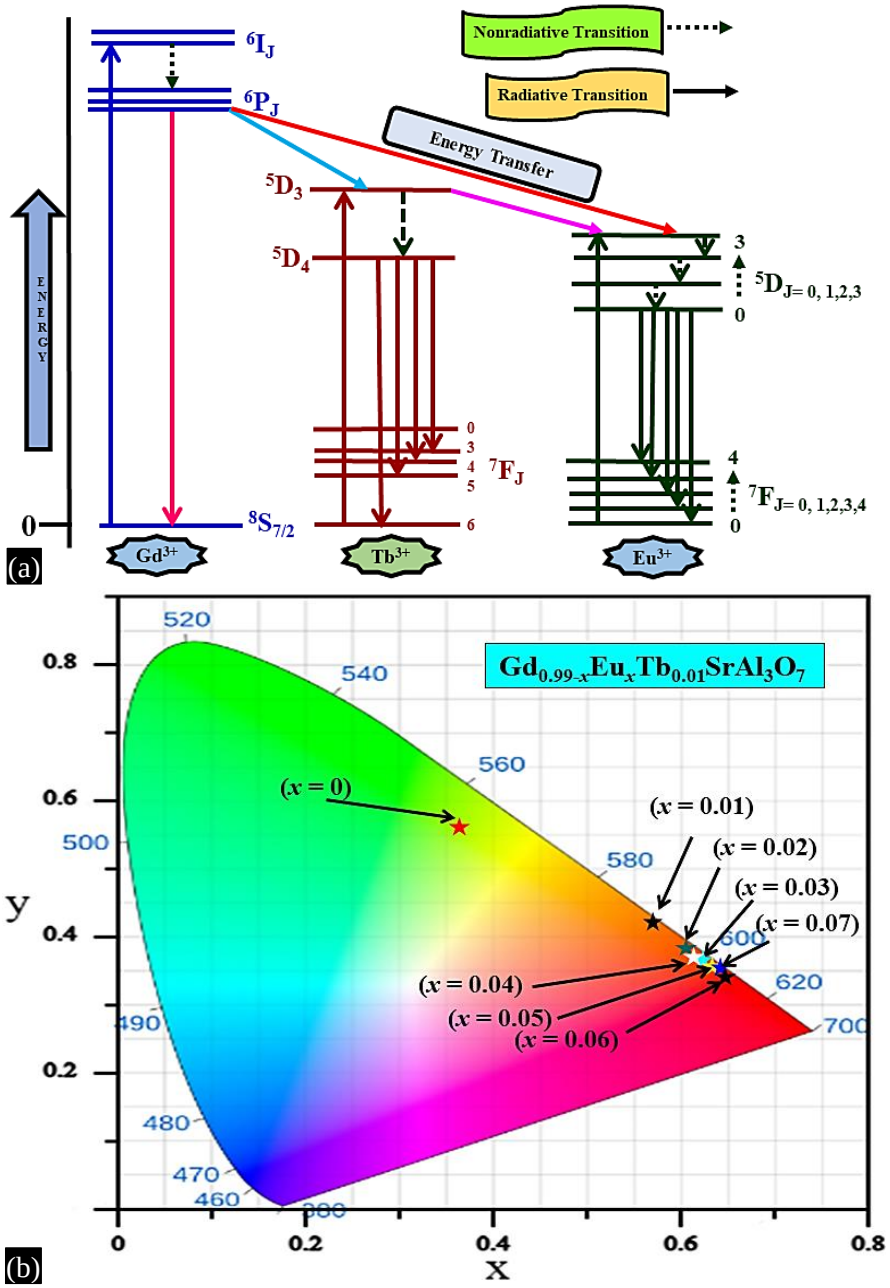

Figure 6. (a) Diagram portraying possible energy transfer process in Eu^{3+}/Tb^{3+} co-doped $GdSrAl_3O_7$ and (b) their CIE color coordinates illustration.

Table 3. Diverse chromaticity metrics of synthesized nanocrystalline phosphors.

Phosphor	(x, y)	CP (%)	(u′, v′)	CCT (K)
$Gd_{0.99}Tb_{0.01}SrAl_3O_7$	(0.367, 0.554)	58.51	0.165, 0.558	-
$Gd_{0.98}Eu_{0.01}Tb_{0.01}SrAl_3O_7$	(0.577, 0.421)	76.08	0.335, 0.549	1783.32
$Gd_{0.97}Eu_{0.02}Tb_{0.01}SrAl_3O_7$	(0.607, 0.391)	81.24	0.375, 0.543	1738.07
$Gd_{0.96}Eu_{0.03}Tb_{0.01}SrAl_3O_7$	(0.629, 0.370)	85.81	0.408, 0.539	1991.44
$Gd_{0.95}Eu_{0.04}Tb_{0.01}SrAl_3O_7$	(0.627, 0.372)	85.37	0.404, 0.539	1954.46
$Gd_{0.94}Eu_{0.05}Tb_{0.01}SrAl_3O_7$	(0.644, 0.355)	89.19	0.431, 0.535	2366.09
$Gd_{0.93}Eu_{0.06}Tb_{0.01}SrAl_3O_7$	(0.647, 0.352)	89.89	0.436, 0.534	2464.50
$Gd_{0.92}Eu_{0.07}Tb_{0.01}SrAl_3O_7$	(0.646, 0.354)	89.68	0.434, 0.535	2414.1

The chromaticity parameters (CCT, CP, and u′, v′) of $Gd_{0.99-x}Eu_xTb_{0.01}SrAl_3O_7$ (x = 0, 0.01 to 0.07 mol) were tabulated in Table 3 along with their CIE coordinates, which were also demonstrated in Figure 6b for assessing the color-tunable of the synthesized nanophosphors.

CONCLUSIONS

In summary, a series of tunable color illuminating pure tetragonal phased Europium (III) and Terbium (III) co-doped of $GdSrAl_3O_7$ nanophosphors were effectively synthesized utilizing easy-to-use, self-propagating urea-supported solution combustion method. Morphological traits were clearly validated agglomeration with spherical-shaped porous particles in nano-regime. The band gap values of the synthesised nanocrystalline phosphors were also derived. Comprehensive luminescence studies were conveyed to validate the color tunable emission in Eu^{3+}/Tb^{3+} co-doped $GdSrAl_3O_7$ nanophosphors. The quadrupole-quadrupole interaction emerged to be responsible for the basis of the non-radiant energy loss phenomenon in directed co-doped nanophosphors. The precisely outlined CIE diagrams illustrated $Gd_{0.99-x}Eu_xTb_{0.01}SrAl_3O_7$ (x = 0, 0.01 to 0.07 mol) nanophosphors samples color hues ranging from light green→ orange → orange-red → dark red with variations in the Eu^{3+}. All the obtained outcomes for the considered co-doped $GdSrAl_3O_7$ phosphors assert their efficacy for cutting-edge luminescent materials that can be used in field emission displays, solid-state technologies, multicolor display applications, photovoltaic devices and a variety of illumination strategies.

REFERENCES

1. Bao A, Yang H, Tao C. Synthesis and luminescent properties of nanoparticles $LaSrAl_3O_7$:Eu, Tb. *Curr Appl Phys*. 2009; 9: 1252. doi:10.1016/j.cap.2009.02.008
2. Sheetal, Taxak VB, Mandeep, et al. Synthesis, characterization and luminescent properties of Eu/Tb-doped $LaSrAl_3O_7$ nanophosphors. *J Alloys Compd*. 2013; 549: 135. doi:10.1016/j.jallcom.2012.09.033
3. Naman. Review of bottom-up and top-down nanofabrication techniques. *RP Curr Trends Appl Sci*. 2023; 2: 73. doi:https://researchplateau.com/uploads/reasearchpapers/1694873319.pdf
4. Kumar D, Sharma SK, Verma S, et al. A short review on rare earth doped $NaYF_4$ upconverted nanomaterials for solar cell applications. *Mater. Today Proc.* 2020; 21: 1868. https://doi.org/10.1016/j.matpr.2020.01.243
5. Kumar V, Ntwaeaborwa OM, Soga T, et al. Rare earth doped zinc oxide nanophosphor powder : A future material for solid state lighting and solar cells. *ACS Photonics.* 2017; 4: 2613. https://doi.org/10.1021/acsphotonics.7b00777
6. Akman E, Akin S, Ozturk T, et al. Europium and terbium lanthanide ions co-doping in TiO_2 photoanode to synchronously improve light-harvesting and open-circuit voltage for high- effi ciency dye-sensitized solar cells. *Sol. Energy.* 2020; 202: 227. https://doi.org/10.1016/j.solener.2020.03.108
7. Han Z, Son S, Optimizing the performance of three-dimensional nitrogen- doped graphene supercapacitors by regulating the nitrogen doping concentration. *J. Korean Inst. Electr. Electron. Mater. Eng.* 2023; 36: 376. https://doi.org/10.4313/JKEM.2023.36.4.8
8. Li FT, Ran J, Jaroniec M, et al. Solution combustion synthesis of metal oxide nanomaterials for energy storage and conversion. *Nanoscale.* 2015; 7: 17590. https://doi.org/10.1039/c5nr05299h
9. Skakle JMS, Herd R. Crystal chemistry of $(RE,A)_2M_3O_7$ compounds (RE = Y, lanthanide; A = Ba, Sr, Ca; M = Al, Ga). *Powder Diffr*. 1999; 14: 195. doi:10.1017/S0885715600010526
10. Singh S, Khatkar SP, Boora P, et al. Structural and luminescent properties of Eu^{3+}-doped $GdSrAl_3O_7$ nanophosphor. *J Mater Sci*. 2014; 49: 4773. doi:10.1007/s10853-014-8176-5
11. Bao A, Tao C, Yang H. Luminescent properties of nanoparticles $LaSrAl_3O_7$: RE^{3+} (RE = Eu, Tb) via the citrate sol-gel method. *J Mater Sci Mater Electron*. 2008; 19: 476. doi:10.1007/s10854-007-9366-6
12. Zhou L, Choy WCH, Shi J, et al. Synthesis and luminescent properties of $GdSrAl_3O_7$:Tb^{3+} phosphor under VUV/UV excitation. *J Alloys Compd*. 2008; 463: 302. doi:10.1016/j.jallcom.2007.09.002
13. Mendhe MS, Bhure PP, Dhabale PC, et al. Improvement of luminescence properties of $LaSrAl_3O_7$:Eu^{3+} phosphor. *Mater Today Proc*. 2019; 15: 633. doi:10.1016/j.matpr.2019.04.131

14. Singh V, Watanabe S, Rao TKG, et al. Synthesis, characterization, luminescence and defect centres in $CaYAl_3O_7:Eu^{3+}$ red phosphor. *J Fluoresc*. 2011; 21: 313. doi:10.1007/s10895-010-0718-x
15. Khatkar SP, Singh S, Lohra S, et al. Photoluminescent properties of Tb^{3+} doped $GdSrAl_3O_7$ nanophosphor using solution combustions synthesis. *Electron Mater Lett*. 2015; 11: 409. doi:10.1007/s13391-014-3293-5
16. Dhaterwal D, Matoria M, Dalal A, et al. Synthesis and characterization of color tunable europium(III) and terbium(III) co-doped $LaSrAl_3O_7$ nanocrystalline phosphors: A photoluminescent synergy. *Asian J Chem*. 2024; 36: 1933. doi:10.14233/ajchem.2024.32115
17. Dhaterwal D, Singh S. A review study on the structural and photoluminescence properties of rare earth doped lanthanate ALa_2ZnO_5 (A = Ca, Sr or Ba) phosphors. *Materialia*. 2021; 20: 101249. doi:10.1016/J.MTLA.2021.101249
18. Kumar P, Singh D, Gupta I, et al. Structural and luminescent characteristics of orthorhombic $GdAlO_3:Sm^{3+}$ nanocrystalline materials for solid state lighting. *Chem Phys Lett*. 2023; 812: 140277. doi:10.1016/j.cplett.2022.140277
19. Sehrawat P, Malik RK, Boora P, et al. Multicolor luminescence evolving from single-phase Eu^{3+}/Tb^{3+} co-doped $SrLaAlO_4$ nanomaterials for advanced photonic appliances. *Chem Phys Lett*. 2021; 763: 138243. doi:10.1016/j.cplett.2020.138243
20. Kumar P, Singh D, Gupta I, et al. Cool green light emitting $GdAlO_3:Tb^{3+}$ perovskite nanomaterials: Crystal structure and spectroscopic characteristics for advance display appliances. *Inorg Chem Commun*. 2022; 145: 110064. doi:10.1016/j.inoche.2022.110064
21. Dhaterwal D, Matoria M, Dalal A, et al. Synthesis and structural features of tunable emitting single-phased Eu^{3+}/Tb^{3+} co- doped $LaAlO_3$ nanophosphors. *J Struct Chem*. 2024; 65: 130877. doi:10.26902/JSC_id130877
22. Shilpa CJ, Jayaram AK, Dhananjaya N, et al. $GdAlO_3:Eu^{3+}:Bi^{3+}$ nanophosphor: Synthesis and enhancement of red emission for WLEDs. *Spectrochim Acta - Part A Mol Biomol Spectrosc*. 2014; 133: 550. doi:10.1016/j.saa.2014.05.082
23. Premkumar HB, Sunitha DV, Nagabhushana H, et al. Synthesis, structural and thermoluminescence properties of $YAlO_3:Dy^{3+}$ nanophosphors. *J Alloys Compd*. 2014; 591: 337. doi:10.1016/j.jallcom.2013.12.217
24. Singh N. Synthesis by precipitation method and investigation of SnO_2 nanoparticles. *RP Curr Trends Appl Sci*. 2023; 2: 30. doi:https://researchplateau.com/uploads/reasearchpapers/1693820785.pdf
25. Surila. Synthesis and characterization of nanosize particles of hematite by sol-gel technique. *RP Curr Trends Eng Technol*. 2023; 2: 1. doi:https://researchplateau.com/uploads/reasearchpapers/1678003280.pdf
26. Jisha PK, Naik R, Prashantha SC, et al. Facile combustion synthesized orthorhombic $GdAlO_3:Eu^{3+}$ nanophosphors: Structural and photoluminescence properties for WLEDs. *J Lumin*. 2015; 163: 47. doi:10.1016/j.jlumin.2015.03.006
27. Zhang Y, Zhang X, Zhang H, et al. Tunable emission from green to red in the $GdSr_2AlO_5:Tb^{3+}$, Eu^{3+} phosphor: Via efficient energy transfer. *RSC Adv*. 2018; 8: 3530. doi:10.1039/c7ra12260h
28. Prasad M, Rai VK. Thermally stable upconverting $Na_3Zr_2(SiO_4)_2PO_4:Er^{3+}/Yb^{3+}$ phosphors for displays and optical thermometry. *J Alloys Compd*. 2022; 911: 164968. doi:10.1016/j.jallcom.2022.164968
29. Kubelka P. New contributions to the optics of intensely light-scattering materials. Part I. *J Opt Soc Am*. 1954; 44: 330. doi:10.1364/JOSA.44.000330
30. Mahajan R, Prakash R. Effect of Sm^{3+} doping on optical properties of $Mg_2P_2O_7$ and $Mg_3P_2O_8$ phosphors. *Mater Chem Phys*. 2020; 246: 122826. doi:10.1016/j.matchemphys.2020.122826
31. Venugopal M, Kumar HP, Jayakrishnan R. Synthesis, characterization and photoluminescent properties of Sm^{3+}/Dy^{3+} doped strontium zirconate perovskites. *J Electroceramics*. 2020; 44: 163. doi:10.1007/s10832-020-00207-6
32. Krishnapriya T, Jose A, Anna Jose T, et al. Luminescent kinetics of Dy^{3+} doped $CaZn_2(PO_4)_2$ phosphors for white light emitting applications. *Adv Powder Technol*. 2021; 32: 1023. doi:10.1016/j.apt.2021.02.003

33. Kumar P, Singh D, Gupta I, et al. Er^{3+}-doped $Y_4Al_2O_9$ nanophosphors for advance display applications: Synthesis, crystal chemistry and down conversion photoluminescent investigation. *Mater Chem Phys*. 2023; 301: 127610. doi:10.1016/j.matchemphys.2023.127610
34. Upadhyay K, Tamrakar RK, Dubey V. High temperature solid state synthesis and photoluminescence behavior of Eu^{3+} doped $GdAlO_3$ nanophosphor. *Superlattices Microstruct*. 2015; 78: 116. doi:10.1016/j.spmi.2014.11.030
35. Oliveira HHS, Cebim MA, Da Silva AA, et al. Structural and optical properties of $GdAlO_3:RE^{3+}$ (RE = Eu or Tb) prepared by the Pechini method for application as X-ray phosphors. *J Alloys Compd*. 2009; 488: 619. doi:10.1016/j.jallcom.2009.04.099
36. Shen B, Wu F, Zhang Y, et al. Multicolour emission from thermally stable Tb^{3+}/Eu^{3+} co-doped $CaLa_4Si_3O_{13}$ phosphors for single-component w-LEDs application. *J Alloys Compd*. 2019; 809: 151836. doi:10.1016/j.jallcom.2019.151836
37. Li G, Wang Y, Wei Y, et al. Structure, energy transfer, and luminescence properties of $NaLaMgWO_6$:-Tb^{3+}, Eu^{3+} phosphors for solid-state lighting. *J Mater Sci Mater Electron*. 2020; 31: 3835. doi:10.1007/s10854-020-02918-6
38. Xu MJ, Si JY, Li GH, et al. Structure, tunable luminescence and thermal stability in Tb^{3+} and Eu^{3+} co-doped novel $KBaIn_2(PO_4)_3$ phosphors. *J Lumin*. 2020; 221: 117115. doi:10.1016/j.jlumin.2020.117115
39. Shaik EB, Kumar BVN, Chirauri SK, et al. Realization of effective energy transfer and color tunability between Tb^{3+} and Eu^{3+} ions in $LaAlO_3$ host for LED display applications. *J Mater Sci Mater Electron*. 2022; 33: 105. doi:10.1007/s10854-021-07257-8
40. Li H, Liu G, Wang J, et al. Eu^{3+}/Tb^{3+} doped cubic $BaGdF_5$ multifunctional nanophosphors: Multicolor tunable luminescence, energy transfer and magnetic properties. *J Lumin*. 2017; 186: 6. doi:10.1016/j.jlumin.2017.02.005
41. Dalal H, Kumar M, Devi S, et al. Crystal configuration and luminescence dynamics of highly efficient green-glimmering vanadate-based $Ca_9Gd(VO_4)_7:Er^{3+}$ nanomaterials pertinent for next-generation illumination applications. *Inorg Chem Commun*. 2023; 151: 110593. doi:10.1016/j.inoche.2023.110593
42. Rawat K, Vishwakarma AK, Jha K. Multicolor emission and energy transfer dynamics in thermally stable $Ca_2Ga_2SiO_7:Tb^{3+}/Eu^{3+}$ for warm w-LEDs application. *Opt Laser Technol*. 2022; 145: 107455. doi:10.1016/j.optlastec.2021.107455
43. Blasse G, Bril A. Energy transfer in Tb^{3+}- activated cerium(III) compounds. *J Chem Phys*. 1969; 51: 3252. doi:10.1063/1.1672503
44. Dexter DL, Schulman JH. Theory of concentration quenching in inorganic phosphors. *J Chem Phys*. 1954; 22: 1063. doi:10.1063/1.1740265
45. Niu J, Sos N, Zhang Z, et al. Tunable emission of $Sr_3Sc(PO_4)_3:Tb^{3+}$, Eu^{3+} phosphors with efficient energy transfer and high thermal stability. *Opt Mater (Amst)*. 2019; 97: 109397. doi:10.1016/j.optmat.2019.109397
46. Xie J, Cheng L, Tang H, et al. Wide range color tunability and efficient energy transfer of novel $NaCaGd(WO_4)_3:Tb^{3+},Eu^{3+}$ phosphors with excellent thermal stability for pc-WLEDs. *Inorg Chem Front*. 2021; 8: 4517. doi:10.1039/d1qi00831e
47. Dhaterwal D, Matoria M, Singh S. Study of the synthesis techniques and photoluminescence properties of Eu^{3+}-Tb^{3+} co-doped phosphors: A review. *Next Nanotechnol*. 2024; 5: 100033. doi:10.1016/j.nxnano.2023.100033
48. Sheoran M, Sehrawat P, Kumari N, et al. Cool white light emanation and photo physical features of combustion derived Dy^{3+} doped ternary yttrate oxide based nanophosphors for down converted WLEDs. *Chem Phys Lett*. 2021; 773: 138608. doi:10.1016/j.cplett.2021.138608
49. Singh S, Dalal A, Kumar M, et al. Structural and luminescence analysis of low temperature solution combustion derived white light emitting $Y_{2(1-x)}Dy_{2x}Zr_2O_7$ nanophosphors for WLEDs. *Asian J Chem*. 2023; 35: 1019. doi:10.14233/ajchem.2023.27019
50. Yashaswini, Pratibha S, Lokesh R, et al. Disaccharide assisted $LaAlO_3:Ce^{3+}$ perovskite: Structural and optical studies suitable for display devices. *Inorg Chem Commun*. 2021; 123: 108342. doi:10.1016/j.inoche.2020.108342

